RESEARCH ARTICLE

ADVANCED
NANOBIOMED
RESEARCH
Open Access

www.advnanobiomedres.com

Fluorescent Nanodiamond–Nanogels for Nanoscale Sensing and Photodynamic Applications

Yingke Wu, Md Noor A Alam, Priyadharshini Balasubramanian, Pia Winterwerber, Anna Ermakova, Michael Müller, Manfred Wagner, Fedor Jelezko,* Marco Raabe,* and Tanja Weil*

Fluorescent nanodiamonds (NDs) are carbon-based nanoparticles with various outstanding magneto—optical properties. After preparation, NDs have a variety of different surface groups that determine their physicochemical properties. For biological applications, surface modifications are crucial to impart a new interface for controlled interactions with biomolecules or cells. Herein, a straightforward synthesis concept denoted "adsorption—crosslinking" is applied for the efficient modification of NDs, which sequentially combines fast noncovalent adsorption based on electrostatic interactions and subsequent covalent crosslinking. As a result, a very thin and uniform nanogel (NG) coating surrounding the NDs is obtained, which imparts reactive groups as well as high colloidal stability. The impact of the reaction time, monomer concentration, molecular weight, structure of the crosslinker on the resulting NG shell, the availability of reactive chemical surface functions, and the quantum sensing properties of the coated NDs are assessed and optimized. Postmodification of the NG-coated NDs is achieved with phototoxic ruthenium complexes yielding ND-based probes suitable for photodynamic applications. The adsorption—crosslinking ND functionalization reported herein provides new avenues toward functional probes and traceable nanocarriers for high-resolution bioimaging, nanoscale sensing, and photodynamic applications.

1. Introduction

Among many carbon-based nanoscale materials, fluorescent nanodiamonds (NDs) have emerged for diverse applications in nanomedicine and bioimaging, because of their unique magneto—optical properties as well as their high biocompatibility.[1] The optically active atom defects in the lattice of NDs, such as the nitrogen vacancy (NV) center, provide stable fluorescence without photobleaching or photoblinking.[2] Due to their stable fluorescence, NDs with NV centers have been applied widely in bioimaging,[3] as well as real-time reporters for drug delivery.[4–6] In addition, the emission wavelength of NDs is size independent but tunable from the visible to the near-infrared region based on the color center (e.g., Si, Ge, etc.).[7] Furthermore, NDs containing negatively charged NV (NV⁻) centers can serve as single-spin sensors to detect critical physical parameters in a biological microenvironment, such as temperature,[8] magnetic fields,[9] electron spins,[10] and mechanical strain.[11]

However, for most of these applications, an appropriate surface functionalization of the NDs is essential, because the colloidal stability of unmodified nanosized NDs in physiological buffer systems is extremely poor due to aggregation.[12] Moreover, the shell provides further reactive groups to attach the desired functionalities, such as drug molecules, dyes, cell- or tissue-targeting groups, or various proteins like antibodies.[13] The surface coating shields the inner ND surface and creates a new interface, which is particularly attractive for in vitro or in vivo applications, i.e., to prevent foreign body interactions[14] or increase their circulation times[12] or their accumulation at the target site.[15] In the past, various different ND surface coating materials and strategies have been reported. The covalent attachment of functionalities such as a silica shell,[16] hyperbranched polyglycerols (HPG),[17] poly(L-DOPA),[5] and antibodies[18] has been explored as well as noncovalent adsorption of biomolecules or polymers like polyethyleneimine,[19] insulin,[20] and albumin-based copolymers.[4] Nevertheless, uncontrolled aggregation as well as precipitation still represents a challenge and each reported functionalization strategy has its benefits but also inherent limitations. Covalent conjugation approaches are typically challenged by the low number of

Y. Wu, M. N. A. Alam, P. Winterwerber, Dr. A. Ermakova, M. Müller, Dr. M. Wagner, Dr. M. Raabe, Prof. T. Weil
Department of Synthesis of Macromolecules
Max Planck Institute for Polymer Research
Ackermannweg 10, Mainz 55128, Germany
E-mail: raabe@mpip-mainz.mpg.de; weil@mpip-mainz.mpg.de

M. N. A. Alam, Dr. M. Raabe, Prof. T. Weil
Institute of Inorganic Chemistry I
Ulm University
Albert-Einstein-Allee 11, Ulm 89081, Germany

P. Balasubramanian, Prof. F. Jelezko
Institute for Quantum Optics and IQST
Ulm University
Albert-Einstein-Allee 11, Ulm 89081, Germany
E-mail: fedor.jelezko@uni-ulm.de

The ORCID identification number(s) for the author(s) of this article can be found under https://doi.org/10.1002/anbr.202000101.

**ADVANCED
SCIENCE NEWS**
www.advancedsciencenews.com

**ADVANCED
NANOBIOMED
RESEARCH**
Open Access
www.advnanobiomedres.com

functionalities intrinsically present at the ND surface.[21] Therefore, often only few surface groups could be attached and batch-to-batch variations of the NDs can cause reproducibility problems. ND coating by physical adsorption is a straightforward procedure, which is less influenced by changes of the ND surface groups. However, ligand loss often occurs in biological media, thus limiting the stability of the nanoparticle, i.e., during cell studies.[22] We propose that the combination of both covalent and noncovalent coating approaches offers efficient functionalization and stabilization of NDs.

Herein, we report a straightforward procedure based on the noncovalent adsorption and covalent crosslinking method that imparts a nanogel (NG) shell at the ND surface. First, the adsorption of multifunctional and positively charged ligands precoats the NDs based on electrostatic interactions followed by a crosslinking step to afford a stable and soft NG shell. Hyperbranched polyethyleneimine (PEI) is a highly branched, cationic polymer with multiple primary amino groups that allow cellular uptake by endocytosis, which has been widely used in biomedical applications, such as cell transfection[23] and gene therapy.[24] In addition, to avoid aggregation of NDs during the adsorption of PEI, polyvinylpyrrolidone (PVP) has been applied as a commonly used stabilizer[25] with proven biocompatibility, as demonstrated in biomedical applications such as in tissue engineering.[26] PEI has been crosslinked with poly(ethylene glycol) to generate the soft and homogeneous ND−NG shell, providing high colloidal stability, reactive primary amino groups for postmodifications, and low cellular toxicity. We accomplished a ND−NG platform for the design of ND-based photosensitizers for photodynamic applications. Photodynamic therapy (PDT) is widely applied in skin cancer and here, light energy is converted locally at the tumor site into reactive oxygen species that affect cancer cell viability.[27] In the future, real-time monitoring of the local changes in ion concentration of certain protein markers, i.e., upon drug treatment, could give new insights into cellular processes during therapy. In this way, a traceable ND-based photodynamic agent combining sensing, imaging, and drug delivery offers great prospects for nanomedicine.

2. Results and Discussion

The adsorption and crosslinking procedure to generate a NG shell around NDs is shown in **Figure 1**A. First, the NDs are mixed with hyperbranched polyethyleneimine (PEI, MW: 25 kDa) in the presence of polyvinylpyrrolidone (PVP, MW: 10 kDa) in Milli-Q water. At slightly alkaline (pH 7.4) conditions in the presence of phosphate-buffered saline (PBS), the 4-arm PEG-NHS ester was applied to crosslink the surface-adsorbed PEI for about 90 min. Purification was accomplished by several washing steps to remove unreacted precursors and smaller NGs without the embedded ND to obtain the pure ND−NGs, as shown in Table S1, Supporting Information.

The ND and ND−NGs were characterized with regard to their distribution, shape, and morphology by transmission electron microscopy (TEM; Figure 1B,C). As shown in Figure 1B, TEM images revealed that bare NDs were prone to significant aggregation and displayed a heterogeneous distribution, whereas nonaggregating, homogeneous single particles

could be observed for ND−NGs (Figure 1C). High-resolution transmission electron microscopy (HRTEM) imaging showed a uniform ring of 2 nm surrounding the NDs, indicating the presence of a dry NG coating (Figure S1, Supporting Information). Because the shell was low in contrast and measured under dry conditions by TEM, we further assessed the core−shell structure of the ND−NGs by liquid-mode atomic force microscopy (AFM; Figure 1D,E), in which the NG could swell compared with the dry TEM conditions. In Figure 1D, the topographic image of ND−NGs and deformation images showed good distribution with no obvious aggregation. NanoScope Analysis 1.8 software was used to process the data and visualize the NG coating.[28] Apart from the height profile images, further nanomechanical properties were simultaneously recorded. In particular, the deformation of the sample caused by the probe was analyzed to receive in-depth information on the structure of the coated NDs. As the ND core is much harder than the NG shell, the deformation of the NG shell could be detected with greater intensity under the same stress conditions. The deformation image revealed clearly that all NDs were uniformly surrounded by a soft shell (Figure 1D, right). Furthermore, the deformation image was studied at higher magnification (Figure 1E), and ≈10 nm thickness of the NG was determined in liquid, which is sufficiently thin for nanoscale sensing applications.

The ND−NGs were characterized by dynamic light scattering (DLS) to measure the shell thickness of dispersed ND−NGs in aqueous solution. The average hydrodynamic diameters in Milli-Q water of NDs and ND−NGs were 36.2 ± 2.4 and 57.0 ± 1.2 nm, respectively, resulting in a shell thickness of 10.4 ± 3.6 nm of the ND−NGs ($n = 3$, **Figure 2**A, Table S2 and Figure S3A, Supporting Information). The ND−NGs were also characterized by multiangle light scattering, which is more sensitive to detect aggregation. No aggregate formation was observed and a shell thickness of about 9 nm (Figure S2, Supporting Information) was determined, which are in agreement with the results from the AFM measurements (10 nm). Variation of the reaction conditions on the hydrodynamic diameters of the ND−NGs was investigated by DLS. As shown in Figure S3B, Supporting Information, their sizes increased with the reaction time from 45.7 ± 5.6 to 52.2 ± 4.0 nm. However, the increments slowed down gradually and stabilized after 90 min, suggesting that the reaction reached saturation or completion. When the concentration of the crosslinker was increased from 0.125 to 8 mg mL^{-1}, ND−NGs of 57.0 ± 1.2 nm were obtained with 2 mg mL^{-1} but the sizes subsequently increased to 74.9 ± 9.9 nm for 8 mg mL^{-1} crosslinker. In addition, the PEI concentrations also varied from 0.01 to 10 mg mL^{-1} to assess the influence on the resulting colloidal stability (Figure 2B). Aggregation was detected at a concentration, for ND−NGs, of 0.01 mg mL^{-1}, most likely because the low amount of PEI around single ND was insufficient to impart sufficient colloidal stability. At 1 mg mL^{-1}, ND−NGs with dimensions of about 50.2 ± 6.0 nm were detected, indicating that a sufficient amount of PEI covered the surface of the NDs, thus forming a thin shell. Further increase in PEI to 10 mg mL^{-1} resulted in a significantly thicker shell (160.9 ± 22.6 nm). The influence of the molecular weight (MW) of PEI and a regularly branched polyamidoamine (PAMAM) dendrimer with a globular sphere-like structure
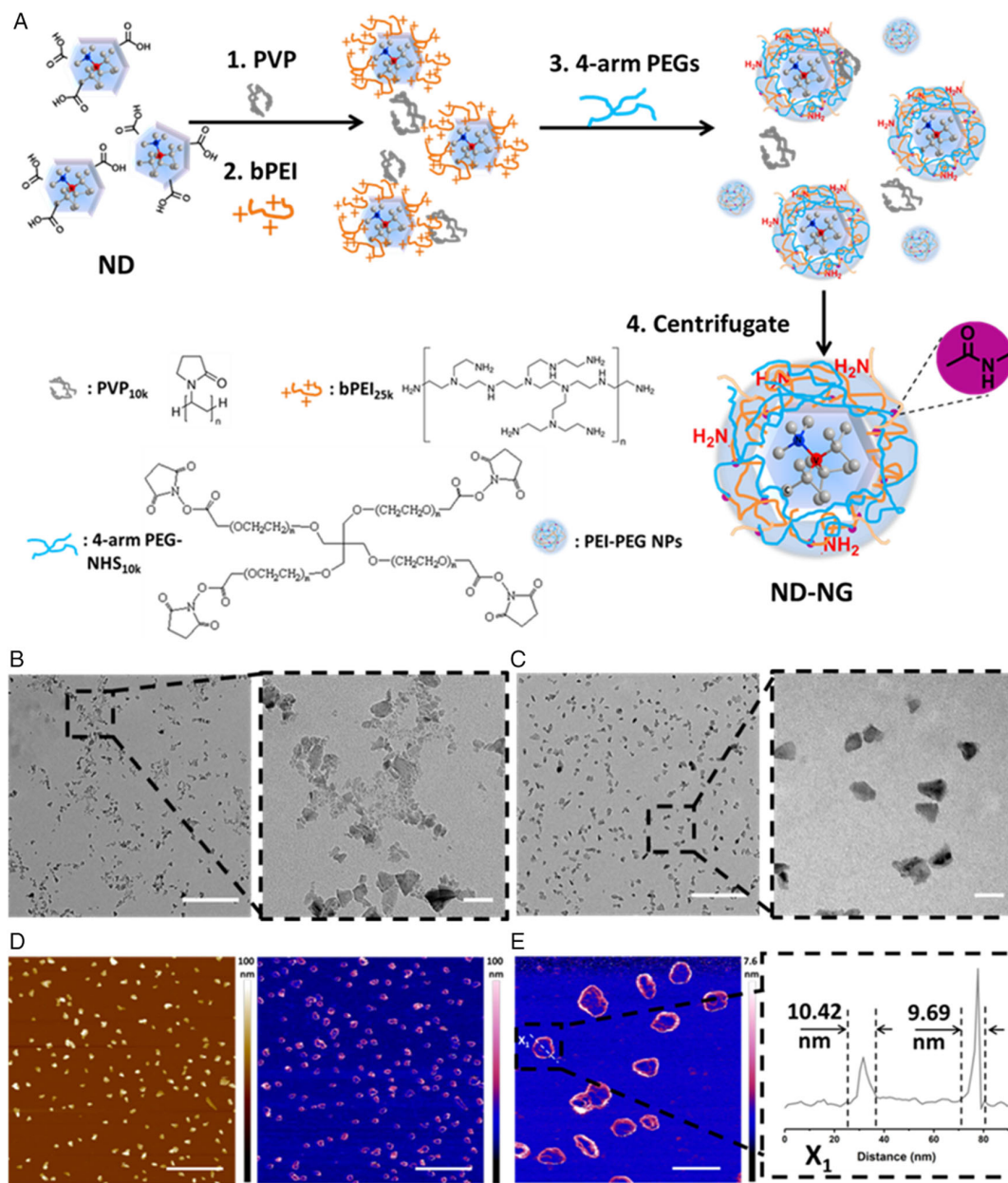
**ADVANCED
SCIENCE NEWS**

www.advancedsciencenews.com

**ADVANCED
NANOBIOMED
RESEARCH**

www.advnanobiomedres.com

Figure 1. A) Schematic illustration of the preparation of ND−NGs. B) TEM images of NDs (left: scale bar = 500 nm; right: scale bar = 50 nm). C) TEM images of ND−NGs (left: scale bar = 500 nm; right: scale bar = 50 nm). D) AFM images of ND−NGs at liquid state (left: height sensor; right: deformation; scale bar = 500 nm). E) AFM images of ND−NGs (left: scale bar = 100 nm; right: deformation distance curve of ND−NGs).

(PAMAM-G3) as well as the buffer, which was used to prepare ND−NGs, was investigated (Figure S4, Supporting Information). NDs aggregated and precipitated when PEIs with lower MW were used (PEI 600 Da and PEI 2000 Da). Alternatives, such as the positively charged dendrimer PAMAM-G3, did not improve colloidal stability, and precipitation was likewise observed, implying that only the positively charged branched polymer with appropriate MW (PEI 25 000 Da) and molecular structure allowed the preparation of stable ND−NGs. The ionic strengths of the buffer affected the preparation of ND−NGs as well (Figure 2A, Table S2, Supporting Information), yielding ND−NGs with various sizes in

Milli-Q water (83.3 ± 11.0 nm), PBS (57.0 ± 1.2 nm), and HEPES (59.6 ± 6.7 nm).

Postfunctionalization allows controlling the chemical, physical, and physiological properties of ND essential for further applications.[12] PEI possesses many amine groups, which are positively charged at physiological pH. Bare NDs have a zeta potential of -37.2 ± 0.6 mV, which increased to about 18.8 ± 0.78 mV (Table S1, Supporting Information) after coating, due to many free primary amino groups located at the ND−NG surface. Fluorescamine is a commonly used fluorogenic reagent for the detection and quantification of amino groups. An excess
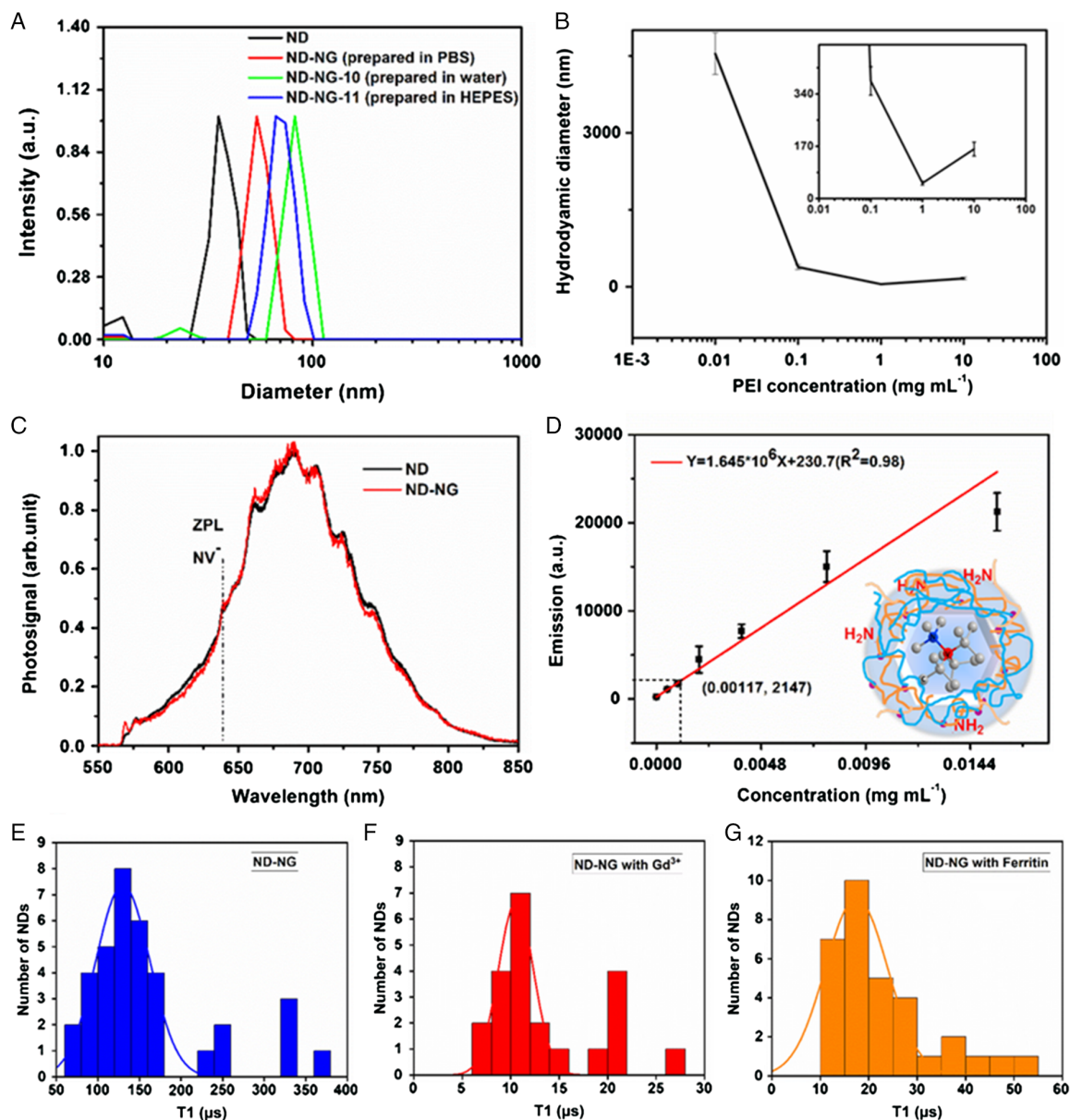
**ADVANCED
SCIENCE NEWS**

www.advancedsciencenews.com

**ADVANCED
NANOBIOMED
RESEARCH**
Open Access

www.advnanobiomedres.com

Figure 2. A) Hydrodynamic diameter of NDs and ND−NGs measured by DLS. B) Influence of the PEI concentration on the size of ND−NGs. Data presented as mean ± SD, $n = 3$. C) Normalized emission spectra (e.g., 532 nm) of NDs and ND−NGs. NV$^-$ zero-phonon lines are visible in both spectra. D) Standard curve of fluorescence intensity using ethylenediamine concentration. Data presented as mean ± SD, $n = 3$. E) T_1 time of ND−NG (129.47 ± 32.5 μs). Data presented as mean ± SD, $n = 37$. F) T_1 time of ND−NG with Gd^{3+} (10.53 ± 1.82 μs). Data presented as mean ± SD, $n = 22$. G) T_1 time of ND−NG with ferritin (17.43 ± 6.45 μs). Data presented as mean ± SD, $n = 34$.

of fluorescamine was added to the ND−NG solution and the fluorescence intensity was measured using an excitation and emission wavelength of 365 and 470 nm (Figure S6, Supporting Information), respectively. In comparison with the control samples, ND−NG, fluorescamine, and water, only the ND−NGs incubated with fluorescamine showed significant fluorescence, proving the accessibility of amino groups present on the surface of ND−NGs. Using ethylenediamine to achieve a calibration plot (Figure 2D), the content of the amine groups on ND−NGs was calculated, suggesting about 3.90×10^{-5} mol primary amino groups (–NH$_2$) per gram ND−NGs. Assuming that

the NDs consist only of C atoms and that all ND−NGs particles have a spherical shape of about 40 nm diameter,[17] this results in an estimated number of about 2769 amino groups per ND−NG that could be used for postmodifications.

The effect of the NG shell on the photophysical properties of NDs containing NV centers was investigated (Figure 2C, Figure S5, Supporting Information). For optical measurements, ND−NGs with a diameter of 57.0 ± 1.2 nm were used. The fluorescence intensity of ND−NGs in water was measured using a laser beam ($\lambda_{ex} = 560$ nm and $\lambda_{em} = 680$ nm, Figure S5, Supporting Information). No significant reduction in the

**ADVANCED
SCIENCE NEWS**
www.advancedsciencenews.com

**ADVANCED
NANOBIOMED
RESEARCH**
Open Access
www.advnanobiomedres.com

fluorescence intensity was observed for ND−NGs compared with bare NDs. In addition, no change in the spectral shape was detected. Furthermore, the effect of the NG shell on the charge state of NV centers in NDs was studied at the single nanoparticle level (Figure 2C). The spectra were measured on a custom-built confocal microscope with an excitation laser at 532 nm and 100 μW power in front of the objective (oil, NA = 1.35). Obviously, the NG shell did not affect the emission properties, and the zero-phonon lines of NV^{-} centers were still well visible without any shift or background noise. NV centers in NDs are very sensitive to the surface states and at some conditions, they can switch to the dark state (neutral NV center; NV^{0} and positively charged NV center; NV^{+}). These results demonstrate that the NG coating did not affect the charge properties of the NV centers, which remained in the optically active states (NV^{-}) and which is important for the future application in bioimaging and nanoscale sensing. To prove the nanoscale sensing ability of ND−NG, Gd^{3+} salt and the iron-storage protein ferritin containing iron in ferric state were selected exemplarily as paramagnetic species. ND−NG was incubated with $GdCl_3$ or ferritin overnight and purified by centrifugation. While the adsorption of ferritin was revealed by TEM (Figure S8A, Supporting Information), Gd^{3+} ions probably penetrated into the NG and were not visible in TEM (Figure S8B + C, Supporting Information). To evaluate the influence of the Gd^{3+} and ferritin adsorbed to ND−NG on the NV spin longitudinal T_1 relaxation time, we used a confocal microscope equipped to conduct T_1 spin relaxometry. A pulsed T_1 sequence was chosen, consisting of repetitive laser pulses in the absence of a microwave. The spin relaxation from the $m_s = 0$ spin state to the thermally mixed state was probed and the relaxometry measurements were carried out on randomly selected single particles (Figure S9, Supporting Information). For each sample, the resulting T_1 constants were averaged. The T_1 time decreased from $129.47 \pm 32.5\,\mu s$ of ND−NG to $10.53 \pm 1.82\,\mu s$ of ND−NG with complexed Gd^{3+} and $17.43 \pm 6.45\,\mu s$ of ND−NG with ferritin, indicating that the ND−NGs are in principle able to sense magnetic fields in their direct surrounding (Figure 2E−G).

Next, the biocompatibility of ND−NGs was investigated using A549 human lung adenocarcinoma cell line (**Figure 3**). As shown in Figure 3B,C, and Figure S7A, Supporting Information, ND−NGs were efficiently taken up into A549 cells after 4 h of incubation. We found many homogenously distributed spherical structures, indicating that ND−NGs were located in intracellular vesicles. The uptake was dependent on the ND−NG concentration and incubation time. When we increased the incubation time from 6 to 24 h and the concentration of ND−NGs from 100 to $200\,\mu g\,mL^{-1}$, the uptake became even more prominent. In addition, cells proliferated well and the cell morphology was not altered. Low cytotoxicity of ND−NGs was observed after the treatment of the cells with a concentration up to $800\,\mu g\,mL^{-1}$ (Figure 3A).

To further evaluate the biocompatibility of ND−NG, the Hen's Egg Test on the Chorioallantoic Membrane (HET-CAM) method[29] was chosen, a potential alternative of animal experiments. The wide availability of fertile eggs and easily achievable hatching temperature (37–38 °C) made the HET-CAM a desirable experiment platform. CAM has an ample vascular network, which is suitable for studying tissue xenograft, tumor growth,

drug delivery, wound healing, and toxicologic study.[30] CAM is not innervated, and the chick embryo develops a functional brain only on day 13 of incubation.[31] Therefore HET-CAM model can be considered as an animal-friendly and humane alternative of in vivo testing. In our HET-CAM test, we observed hemorrhage from blood vassals within 2–4 s after applying the positive control (1% sodium dodecyl sulfate; SDS). Lysis occurred after 25–27 s, and we observed coagulation within 24 h. For the negative control (phosphate-buffered saline) and various concentrations of NG−NG (100, 400, $800\,\mu g\,mL^{-1}$), no instance of irritation was detected from 5 min to 24 h of application (Figure 3D and Figure S7B, Supporting Information). A summary of the results is shown in Table S3, Supporting Information. These in ovo results support the biocompatibility of ND−NG.

To underline the potential of ND−NGs as a theranostic platform, a PDT agent, [4-(1H-imidazo[4,5-f][1,10]phenantholin-2-yl-κN7,κN8)benzoato]-bis(2,2′-bipyridine-κN1,κN1′)ruthenium(1+) chloride (Ru−COOH), was conjugated with the ND−NGs by the reaction of its carboxylic acid with the amine groups of ND−NGs in the presence of EDC to afford ND−NG−Ru (**Figure 4**A). PDT is a treatment using photosensitizing agents, whose bioactivity is activated by light.[32] The photosensitizer produces reactive oxygen species, i.e., singlet oxygen ($^1O_2$) for therapeutic purposes. Singlet oxygen is cytotoxic, which strongly decreases, i.e., viability of tumor cells.[33] PDT is minimally invasive compared with other treatment procedures (e.g., surgery) and can be used together with other therapeutic techniques. Due to the low invasiveness of this approach, small or no scarring at the application site after healing represents an additional benefit for the patient's quality of life. However, there are some drawbacks including low tumor specificity, inefficient cellular uptake, and higher activation energies (if required), leading to prolonged illumination times. To overcome these challenges, ND−NG was used as a carrier system. After modification with Ru−COOH, the attenuated total reflection Fourier-transform infrared (ATR-FTIR) spectrum of ND−NG−Ru was measured (Figure S10, Supporting Information) and this showed that the peak intensity of the stretching vibration of N−H decreased as the amine group reacted with the carboxylic acid groups of Ru−COOH. To quantify the number of Ru complexes on ND−NG−Ru, the fluorescence intensity was measured using an excitation and emission wavelength of 460 and 610 nm, respectively. In comparison with the control samples (ND−NG), only ND−NG−Ru showed emission properties in the characteristic range (Figure S11, Supporting Information). Using a series of Ru−COOH solutions, a calibration plot was generated (Figure 4B) and the content of the Ru complexes on the ND−NG−Ru was calculated to be $3.78\,\mu g\,mg^{-1}$ of ND−NGs. The DLS and TEM measurements of ND−NG−Ru revealed a high colloidal stability with good dispersion and stability in aqueous media (Figure S12 and S13, Supporting Information). Compared with the hydrodynamic size of ND−NG, the dimension of ND−NG−Ru increased from 57.0 ± 1.2 to 73.7 ± 4.9 nm, respectively. In addition, no significant aggregation was observed in TEM images. PDT relies on the efficient production of singlet oxygen in cellular environments. To monitor the generation of $^1O_2$ in a quantitative fashion, we conducted $^1O_2$ production efficiency tests as reported previously.[34] The singlet oxygen sensor 9,10-anthracenediyl-bi(methylene)dimalonic acid (ABDA) was used, which forms an
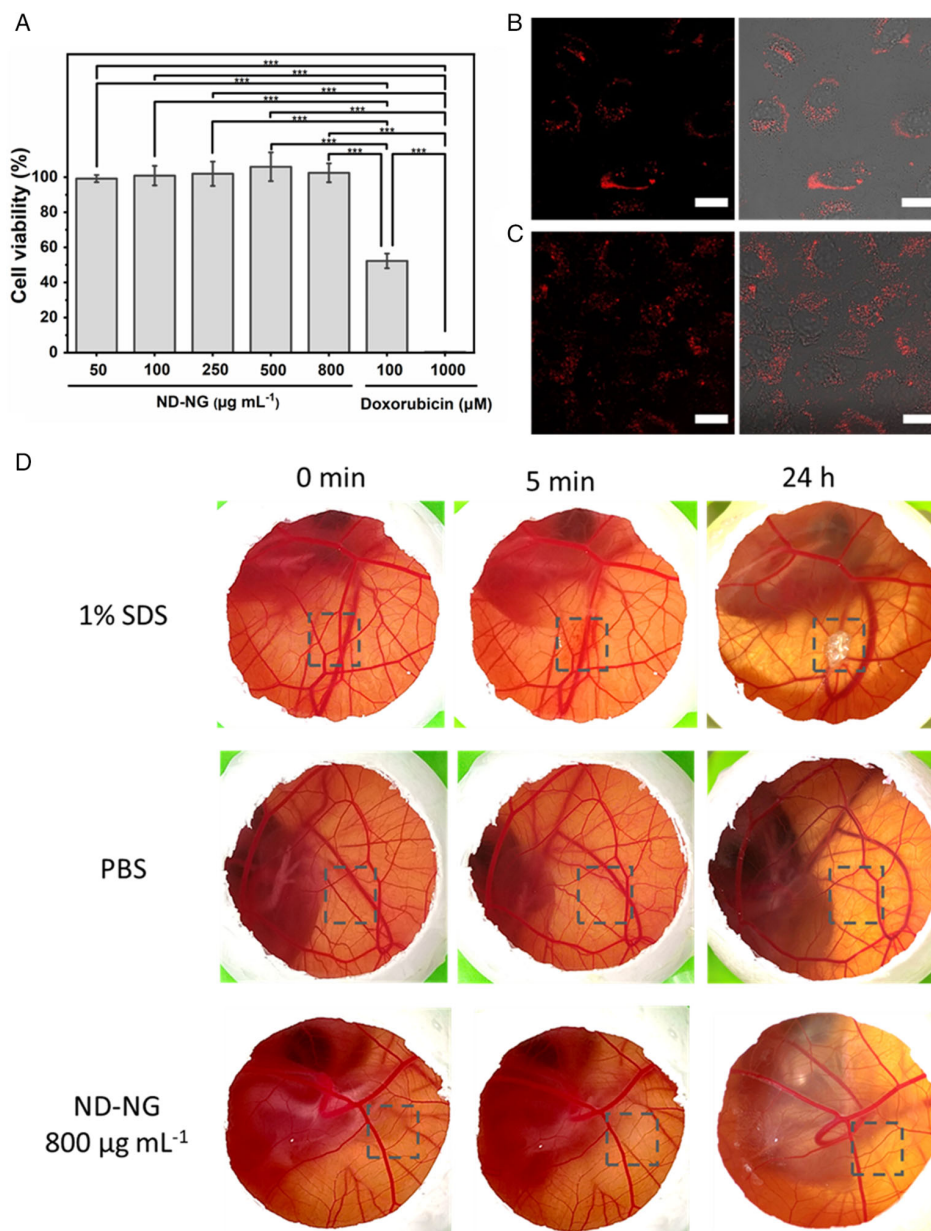
**ADVANCED
SCIENCE NEWS**

www.advancedsciencenews.com

**ADVANCED
NANOBIOMED
RESEARCH**
Open Access

www.advnanobiomedres.com

Figure 3. A) Cell viability in A549 cells with various concentrations of ND−NG, $n = 5$, one-way ANOVA with Tukey's posthoc test, ***$p < 0.001$. All ND−NG concentrations are statistically nonsignificant. B,C) Confocal microscopy images of ND−NGs taken up into A549 cells (scale bar = 20 μm) (B) at 100 μg mL^{-1} for 6 h and (C) at 200 μg mL^{-1} for 24 h. D) Photographs of HET-CAM test results for 1% SDS (positive control), PBS (negative control), and ND−NG at 800 μg mL^{-1}.

endoperoxide of ABDA in the presence of $^1O_2$ that alters its absorbance spectrum. Therefore, the production of $^1O_2$ was monitored by measuring this particular change in absorbance of ABDA (Figure 4C, Figure S14, Supporting Information). ND−NG−Ru, ND−NGs, and bare NDs as control were mixed with 100 μM of ABDA and were irradiated with a 470 nm light-emitting diode (LED) array (20 mW cm^{-2}) for 15 min. Relative changes in absorbance confirmed the successful generation of $^1O_2$. We also examined the intracellular localization of ND−NG−Ru in a human cervical cancer cell line (HeLa cells) by laser scanning confocal microscopy. These cells were

incubated with ND−NG−Ru (100 μg mL^{-1}) for about 4 h before images were recorded (Figure 4E). ND−NG−Ru were efficiently taken up and many homogenously distributed spherical structures were observed, suggesting that ND−NGs were mainly located in intracellular vesicles. To evaluate light-induced cellular toxicity, HeLa cells were incubated with 0–200 μg mL^{-1} ND−NG−Ru for 4 h before irradiation with 470 nm LED light for 15 min (50 mW cm^{-2}). The applied power is comparable with the reported photosensitizing drugs.[35] We found a very low IC$_{50}$ of around 23 μg mL^{-1} for the ND−NG−Ru (Figure 4D), which is similar to the reported IC$_{50}$
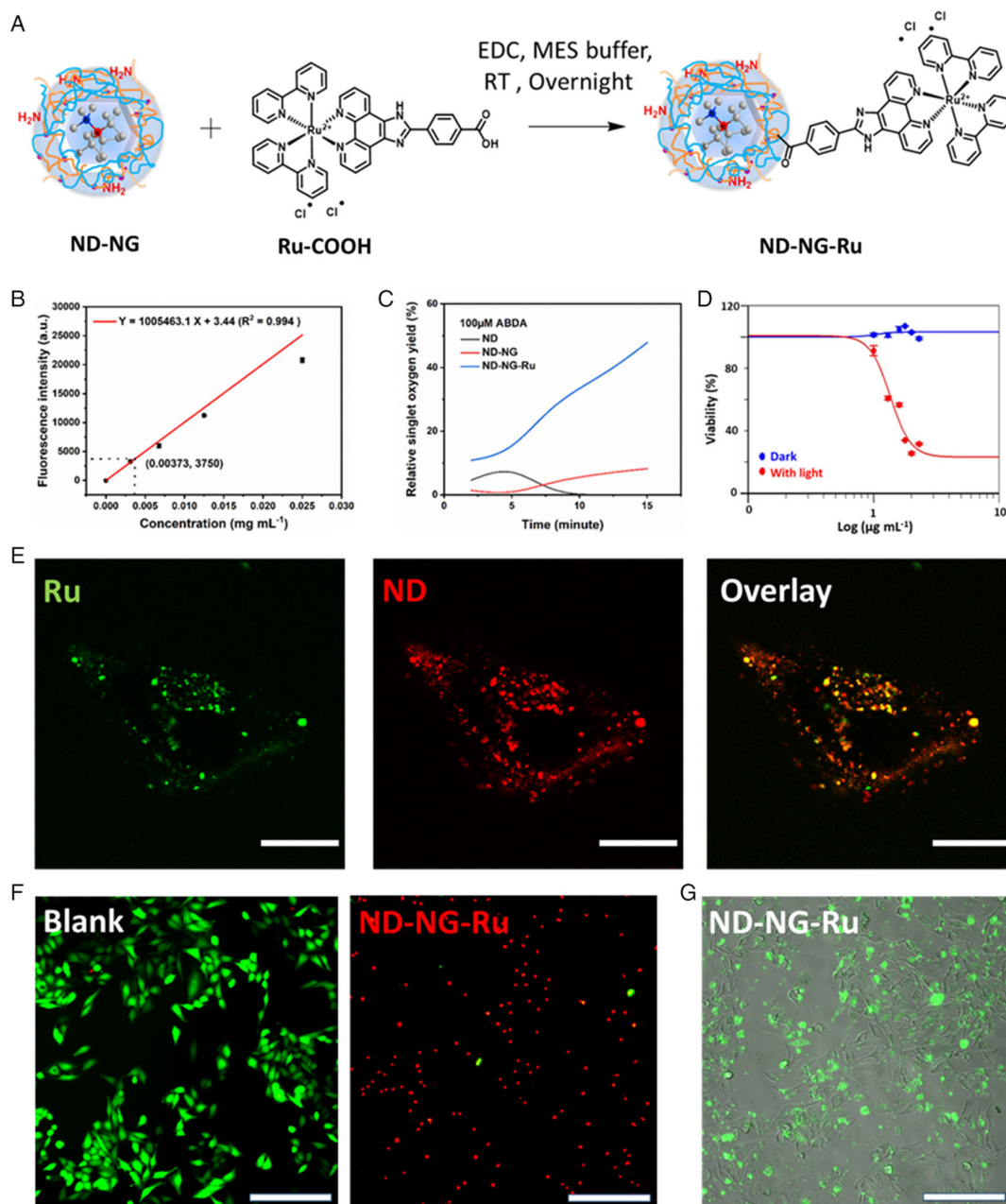
Figure 4. A) Schematic illustration of the preparation of ND−NG−Ru. B) Standard curve of fluorescence intensity using different concentrations of Ru−COOH. Data presented as mean ± SD, $n = 3$. C) Singlet oxygen yield of ND−NG−Ru. D) Logarithmic fitting curve for cell viability of ND−NG−Ru. Data presented as mean ± SD, $n = 3$. E) Confocal microscopy images in HeLa cells after 4 h incubation with 100 µg mL^{-1} ND−NG−Ru (15 min of irradiation, scale bar = 20 µm). Green and red colors represent Ru and ND signal, respectively. F) Live/dead staining of HeLa cells incubated without or with 100 µg mL^{-1} ND−NG−Ru after 15 min of irradiation (scale bar = 200 µm). G) Early apoptosis detection by Annexin V, FITC. Green color represents apoptotic cells (scale bar = 200 µm).

of 15 µg mL^{-1} of the Ru−tetrazole-coordinated nanoparticles.[36] Live/dead staining of the cells using fluorescein diacetate/ propidium iodide further demonstrated that ND−NG−Ru-induced cell death upon irradiation could be spatially controlled (Figure 4F). Furthermore, we confirmed induced cell death using Annexin-V, a protein that binds to phosphatidylserine, which is only present during apoptosis (Figure 4G).

3. Conclusion

In summary, we established the adsorption−crosslinking method as a novel synthesis concept for the surface modification of NDs. This approach combines both noncovalent adsorption and covalent stabilization, thus integrating the advantages of both coating strategies within one system, while overcoming

**ADVANCED
SCIENCE NEWS**

www.advancedsciencenews.com

**ADVANCED
NANOBIOMED
RESEARCH**
Open Access

www.advnanobiomedres.com

their respective drawbacks. Using this method, we successfully prepared ND−NG samples with a thin and uniform NG shell, as well as a narrow size distribution, while elucidating the chemical tools to control its formation. Critically, the photophysical properties of the NV centers in ND were not affected by surface modification, thus facilitating the nanoscale sensing applications. Quantification of the number of amine groups, which are present on the surface of ND−NGs, was achieved. Furthermore, the ND−NGs were well tolerated in cell experiments and in in vivo testing. Introduction of a PDT agent, Ru−COOH, was achieved in a postmodification approach. ND−NG−Ru showed successful photodynamic activity in vitro. By demonstrating the capability to combine multiple functions, i.e., the nanoscale sensing and photodynamic ability, the versatility of the platform was proven. Importantly, the adsorption−crosslinking method can be expanded to other chemical motifs, as reactive groups are still available within the NGs for further modification. We believe that our studies pave the way to customized ND-based nanotheranostics for precise diagnosis and therapy at the subcellular level.

Supporting Information

Supporting Information is available from the Wiley Online Library or from the author.

Acknowledgements

Conflict of Interest

The authors declare no conflict of interest.

Data Availability Statement

The data that supports the findings of this study are available in the supplementary material of this article.

Keywords

[1] a) M. Ibrahim, Y. Xue, M. Ostermann, A. Sauter, D. Steinmueller-Nethl, S. Schweeberg, A. Krueger, M. R. Cimpan, K. Mustafa, *J. Biomed. Mater. Res., Part A* **2018**, *106*, 1697; b) K. Adach, M. Fijalkowski, G. Gajek, J. Skolimowski, R. Kontek, A. Blaszczyk, *Chem.-Biol. Interact.* **2016**, *254*, 156; c) V. Vaijayanthimala, P.-Y. Cheng, S.-H. Yeh, K.-K. Liu, C.-H. Hsiao, J.-I. Chao, H.-C. Chang, *Biomaterials* **2012**, *33*, 7794.

[2] G. Balasubramanian, I. Chan, R. Kolesov, M. Al-Hmoud, J. Tisler, C. Shin, C. Kim, A. Wojcik, P. R. Hemmer, A. Krueger, *Nature* **2008**, *455*, 648.

[3] a) S. Han, M. Raabe, L. Hodgson, J. Mantell, P. Verkade, T. Lasser, K. Landfester, T. Weil, I. Lieberwirth, *Nano Lett.* **2019**, *19*, 2178; b) M. D. Torelli, N. A. Nunn, O. A. Shenderova, *Small* **2019**, *15*, 1902151; c) H. S. Jung, K. J. Cho, Y. Seol, Y. Takagi, A. Dittmore, P. A. Roche, K. C. Neuman, *Adv. Funct. Mater.* **2018**, *28*, 1801252.

[4] Y. Wu, A. Ermakova, W. Liu, G. Pramanik, T. M. Vu, A. Kurz, L. McGuinness, B. Naydenov, S. Hafner, R. Reuter, *Adv. Funct. Mater.* **2015**, *25*, 6576.

[5] S. Harvey, M. Raabe, A. Ermakova, Y. Wu, T. Zapata, C. Chen, H. Lu, F. Jelezko, D. Y. Ng, T. Weil, *Adv. Ther.* **2019**, *2*, 1900067.

[6] a) Y. Zhang, Z. Cui, H. Kong, K. Xia, L. Pan, J. Li, Y. Sun, J. Shi, L. Wang, Y. Zhu, *Adv. Mater.* **2016**, *28*, 2699; b) Z. Cui, Y. Zhang, K. Xia, Q. Yan, H. Kong, J. Zhang, X. Zuo, J. Shi, L. Wang, Y. Zhu, *Nat. Commun.* **2018**, *9*, 1; c) T. K. Ryu, S. W. Baek, R. H. Kang, S. W. Choi, *Adv. Funct. Mater.* **2016**, *26*, 6428.

[7] M. H. Alkahtani, F. Alghannam, L. Jiang, A. Almethen, A. A. Rampersaud, R. Brick, C. L. Gomes, M. O. Scully, P. R. Hemmer, *Nanophotonics* **2018**, *7*, 1423.

[8] a) P. Neumann, I. Jakobi, F. Dolde, C. Burk, R. Reuter, G. Waldherr, J. Honert, T. Wolf, A. Brunner, J. H. Shim, *Nano Lett.* **2013**, *13*, 2738; b) D. A. Simpson, E. Morrisroe, J. M. McCoey, A. H. Lombard, D. C. Mendis, F. Treussart, L. T. Hall, S. Petrou, L. C. Hollenberg, *ACS Nano* **2017**, *11*, 12077; c) T. Sekiguchi, S. Sotoma, Y. Harada, *Biophys. Physicobiol.* **2018**, *15*, 229.

[9] a) A. Ermakova, G. Pramanik, J.-M. Cai, G. Algara-Siller, U. Kaiser, T. Weil, Y.-K. Tzeng, H.-C. Chang, L. McGuinness, M. B. Plenio, *Nano Lett.* **2013**, *13*, 3305; b) T. Zhang, G.-Q. Liu, W.-H. Leong, C.-F. Liu, M.-H. Kwok, T. Ngai, R.-B. Liu, Q. Li, *Nat. Commun.* **2018**, *9*, 1.

[10] a) V. R. Horowitz, B. J. Alemán, D. J. Christle, A. N. Cleland, D. D. Awschalom, *Proc. Natl. Acad. Sci.* **2012**, *109*, 13493; b) R. D. Akiel, X. Zhang, C. Abeywardana, V. Stepanov, P. Z. Qin, S. Takahashi, *J. Phys. Chem. B* **2016**, *120*, 4003.

[11] K. Xia, C.-F. Liu, W.-H. Leong, M.-H. Kwok, Z.-Y. Yang, X. Feng, R.-B. Liu, Q. Li, *Nat. Commun.* **2019**, *10*, 1.

[12] K. van der Laan, M. Hasani, T. Zheng, R. Schirhagl, *Small* **2018**, *14*, 1703838.

[13] J. J. Virgen-Ortíz, J. C. dos Santos, Á. Berenguer-Murcia, O. Barbosa, R. C. Rodrigues, R. Fernandez-Lafuente, *J. Mater. Chem. B* **2017**, *5*, 7461.

[14] L. Zhao, Y.-H. Xu, T. Akasaka, S. Abe, N. Komatsu, F. Watari, X. Chen, *Biomaterials* **2014**, *35*, 5393.

[15] L.-W. Tsai, Y.-C. Lin, E. Perevedentseva, A. Lugovtsov, A. Priezzhev, C.-L. Cheng, *Int. J. Mol. Sci.* **2016**, *17*, 1111.

[16] A. Bumb, S. K. Sarkar, N. Billington, M. W. Brechbiel, K. C. Neuman, *J. Am. Chem. Soc.* **2013**, *135*, 7815.

[17] L. Zhao, T. Takimoto, M. Ito, N. Kitagawa, T. Kimura, N. Komatsu, *Angew. Chem., Int. Ed.* **2011**, *50*, 1388.

[18] X. Q. Zhang, R. Lam, X. Xu, E. K. Chow, H. J. Kim, D. Ho, *Adv. Mater.* **2011**, *23*, 4770.

[19] X.-Q. Zhang, M. Chen, R. Lam, X. Xu, E. Osawa, D. Ho, *ACS Nano* **2009**, *3*, 2609.

[20] R. A. Shimkunas, E. Robinson, R. Lam, S. Lu, X. Xu, X.-Q. Zhang, H. Huang, E. Osawa, D. Ho, *Biomaterials* **2009**, *30*, 5720.

[21] J. Ackermann, A. Krueger, *Carbon* **2020**, *163*, 56.

[22] S. R. Hemelaar, A. Nagl, F. Bigot, M. M. Rodríguez-García, M. P. de Vries, M. Chipaux, R. Schirhagl, *Microchim. Acta* **2017**, *184*, 1001.

[23] a) P. A. Longo, J. M. Kavran, M.-S. Kim, D. J. Leahy, in *Methods in Enzymology*, Vol. *529*, Elsevier, Amsterdam/New York **2013**, 227; b) H. Wang, Q. Li, J. Yang, J. Guo, X. Ren, Y. Feng, W. Zhang, *J. Mater. Chem. B* **2017**, *5*, 1408.

[24] a) Y. H. Kim, J. H. Park, M. Lee, Y.-H. Kim, T. G. Park, S. W. Kim, *J. Controlled Release* **2005**, *103*, 209; b) L. Kong, J. Qiu, W. Sun, J. Yang, M. Shen, L. Wang, X. Shi, *Biomater. Sci.* **2017**, *5*, 258; c) W. Sun, Y. Wang, M. Cai, L. Lin, X. Chen, Z. Cao, K. Zhu, X. Shuai, *Biomater. Sci.* **2017**, *5*, 2468.

[25] a) C. Graf, D. L. Vossen, A. Imhof, A. van Blaaderen, *Langmuir: ACS J. Surf. Colloids* **2003**, *19*, 6693; K. M. Koczkur, S. Mourdikoudis, L. Polavarapu, S. E. Skrabalak, *Dalton Trans.* **2015**, *44*, 17883; b) M. Farahmandjou, S. Honarbakhsh, S. Behrouzinia, *Phys. Chem. Res.* **2016**, *4*, 655.

[26] a) R. Mishra, R. Varshney, N. Das, D. Sircar, P. Roy, *Eur. Polym. J.* **2019**, *119*, 155; b) E. Doğan, P. Tokcan, M. Diken, B. Yilmaz, B. Kizilduman, P. Sabaz, *Adv. Mater. Sci.* **2019**, *19*, 32; c) Y. Guo, Z. Hao, C. Wan, *Tribol. Int.* **2016**, *93*, 214.

[27] F. Heinemann, J. Karges, G. Gasser, *Acc. Chem. Res.* **2017**, *50*, 2727.

[28] R. Garcia, R. Proksch, *Eur. Polym. J.* **2013**, *49*, 1897.

[29] G. Winter, A. B. Koch, J. Löffler, M. Lindén, C. Solbach, A. Abaei, H. Li, G. Glatting, A. J. Beer, V. Rasche, *Cancers* **2020**, *12*, 1248.

[30] A. Vargas, M. Zeisser-Labouèbe, N. Lange, R. Gurny, F. Delie, *Adv. Drug Delivery Rev.* **2007**, *59*, 1162.

[31] E. Aleksandrowicz, I. Herr, *ALTEX-Altern. Animal Exp.* **2015**, *32*, 143.

[32] M. C. DeRosa, R. J. Crutchley, *Coord. Chem. Rev.* **2002**, *233*, 351.

[33] T. J. Dougherty, C. J. Gomer, B. W. Henderson, G. Jori, D. Kessel, M. Korbelik, J. Moan, Q. Peng, *JNCI, J. Natl. Cancer Inst.* **1998**, *90*, 889.

[34] T. Wang, N. Zabarska, Y. Wu, M. Lamla, S. Fischer, K. Monczak, D. Y. Ng, S. Rau, T. Weil, *Chem. Commun.* **2015**, *51*, 12552.

[35] S. Chakrabortty, B. K. Agrawalla, A. Stumper, N. M. Vegi, S. Fischer, C. Reichardt, M. Kögler, B. Dietzek, M. Feuring-Buske, C. Buske, *J. Am. Chem. Soc.* **2017**, *139*, 2512.

[36] B. Wei, M. Y. Guo, Y. M. Lu, P. P. Sun, G. W. Yang, Q. Y. Li, *Anorg. Allg. Chem.* **2018**, *644*, 6.